

# The UV properties of E+A galaxies: constraints on feedback-driven quenching of star formation

S. Kaviraj,<sup>1\*</sup> L. A. Kirkby,<sup>1</sup> J. Silk<sup>1</sup> and M. Sarzi<sup>2</sup>

<sup>1</sup>*Department of Physics, University of Oxford, Keble Road, Oxford OX1 3RH*

<sup>2</sup>*Centre for Astrophysics Research, University of Hertfordshire, Hatfield AL10 9AB*

Accepted 2007 September 14. Received 2007 September 14; in original form 2007 July 24

## ABSTRACT

We present the first large-scale study of E+A galaxies that incorporates photometry in the ultraviolet (UV) wavelengths. E+A galaxies are ‘post-starburst’ systems, with strong Balmer absorption lines indicating significant recent star formation, but without [O II] and H $\alpha$  emission lines which are characteristic of ongoing star formation. The starburst that creates the E+A galaxy typically takes place within the last Gyr and creates a high fraction (20–60 per cent) of the stellar mass in the remnant over a short time-scale ( $<0.1$  Gyr). We find a tight correlation between the luminosity of our E+A galaxies and the implied star formation rate (SFR) during the starburst. While low-luminosity E+As [ $M(z) > -20$ ] exhibit implied SFRs of less than  $50 M_{\odot} \text{ yr}^{-1}$ , their luminous counterparts [ $M(z) < -22$ ] show SFRs greater than 300 and as high as  $2000 M_{\odot} \text{ yr}^{-1}$ , suggesting that luminous and ultra-luminous infrared galaxies in the low-redshift Universe could be the progenitors of massive nearby E+A galaxies. We perform a comprehensive study of the characteristics of the quenching that truncates the starburst in E+A systems. We find that, for galaxies less massive than  $10^{10} M_{\odot}$ , the *quenching efficiency* decreases as the galaxy mass increases. However, for galaxies more massive than  $10^{10} M_{\odot}$ , this trend is reversed and the quenching efficiency increases with galaxy mass. Noting that the mass threshold at which this reversal occurs is in excellent agreement with the mass above which active galactic nuclei (AGN) become significantly more abundant in nearby galaxies, we use simple energetic arguments to show that the bimodal behaviour of the quenching efficiency is consistent with AGN and supernovae (SN) being the principal sources of negative feedback above and below  $M \sim 10^{10} M_{\odot}$ , respectively. The arguments assume that quenching occurs through the mechanical ejection or dispersal of the gas reservoir and that, in the high-mass regime ( $M > 10^{10} M_{\odot}$ ), the Eddington ratios in this sample of galaxies scale as  $M^{\gamma}$ , where  $1 < \gamma < 3$ . Finally, we use our E+A sample to estimate the time it takes for galaxies to migrate from the blue cloud to the red sequence. We find migration times between 1 and 5 Gyr, with a median value of 1.5 Gyr.

**Key words:** galaxies: elliptical and lenticular, cD – galaxies: evolution – galaxies: formation – galaxies: fundamental parameters.

## 1 INTRODUCTION

‘E+A’ galaxies exhibit strong Balmer absorption lines, characteristic of significant recent star formation, but lack [O II] or H $\alpha$  emission which are characteristics of ongoing star formation. Their spectral features indicate that a vigorous episode of recent star formation in these systems has been quenched abruptly. As ‘post-starburst’ systems, E+A galaxies provide a valuable evolutionary link between the gas-rich star-forming population and gas-poor quiescent

systems. The persistent dichotomy in galaxy colours over a large range in redshift, coupled with the gradual build-up of the red sequence over time (e.g. Bell et al. 2004), indicates that *how* and *over what time-scale* galaxies evolve from the ‘blue cloud’ to the ‘red sequence’ is of significant importance in understanding the macroscopic evolution of the galaxy population over the lifetime of the Universe. The characteristics of E+A galaxies provide a unique (but transient!) window into the very point where this transition from blue cloud to red sequence is about to begin. Understanding what drives their vigorous star formation episode and, in particular, what causes it to be quenched so suddenly is clearly an important step in our understanding of galaxy evolution.

\*E-mail: skaviraj@astro.ox.ac.uk

First noted by Dressler & Gunn (1983) in distant ( $z \sim 0.4$ ) clusters, E+A galaxies have been subsequently found to be abundant in all types of environments. At intermediate redshifts ( $0.3 < z < 1$ ), the proportion of E+A galaxies appears to be a factor of 4 greater in clusters than in the field (Tran et al. 2004). In the nearby Universe, E+A galaxies have been detected mainly in the field (Zabludoff et al. 1996; Quintero et al. 2004) primarily because most galaxies do not reside in dense cluster-like environments. Indeed, the overall distribution of the local environments of E+A systems follows that of the general galaxy population as a whole (Blake et al. 2004). The fraction of E+A systems in clusters shows a rapid decline from intermediate redshifts ( $z \sim 0.5$ ) where it is typically higher than 20 per cent (e.g. Couch & Sharples 1987; Belloni et al. 1995) to less than 1 per cent in local clusters (Fabricant, McClintock & Bautz 1991).

Several plausible explanations for the E+A phenomenon have been proposed and studies indicate that there are multiple channels for creating such post-starburst spectral signatures. Since E+A galaxies were first detected in clusters, it was initially thought that their production required a cluster-specific mechanism, such as galaxy harassment or ram-pressure stripping. However, their abundant presence in the field indicates that other channels exist for the production of E+A systems (e.g. Goto 2005), although cluster-specific mechanisms may contribute or even dominate their evolutionary pathways in dense regions of the Universe.

Another possible explanation for E+A-like spectra is that the optical emission lines are heavily suppressed by dust obscuration (e.g. Couch & Sharples 1987; Smail et al. 1999; Poggianti & Wu 2000). An efficient test of this scenario is to observe the E+A population in the radio wavelengths where the effects of dust obscuration are absent. However, a radio study of 15 galaxies in the Zabludoff et al. (1996) sample by Miller & Owen (2001) detected only two at radio luminosities which are consistent with modest levels of star formation. Similarly, Goto (2004) performed Very Large Array (VLA) 20-cm radio-continuum observations of 36 E+A galaxies drawn from the Sloan Digital Sky Survey (SDSS) and found that none of these galaxies was detected in the radio wavelengths. These results are supported by Galaz (2000) who does not find compelling evidence for strong internal dust extinction in their E+A sample.

Some E+A galaxies exhibit morphological disturbances indicative of interactions with near neighbours. Yang et al. (2004) have studied the morphologies of the five bluest E+A galaxies in the sample of Zabludoff et al. (1996) using the WFPC2 camera on board the *Hubble Space Telescope* (*HST*) and found that four out of these five galaxies display morphological disturbances consistent with recent mergers. Similarly, Goto (2004) have shown, using the largest sample of E+A galaxies studied to date, that these systems have an excess of local galaxy density at spatial scales less than 100 kpc but not at scales spanned by galaxy clusters ( $\sim 1$  Mpc) or large-scale structure ( $\sim 8$  Mpc). They find that  $\sim 30$  per cent of E+A galaxies exhibit morphological disturbances, indicating that their evolution is linked, at least partially, to mergers and interactions. It is worth noting that, although the Goto (2004) sample is larger and their results are statistically more robust, detection of small, low-surface brightness (tidal) features probably requires both deeper and higher resolution imaging than that provided by the SDSS. Hence, the fraction of E+A galaxies with tidal tails may well be higher than  $\sim 30$  per cent in the Goto (2004) sample, making the conclusions from these two studies more consistent.

From a theoretical perspective, the merger hypothesis is supported by numerical simulations which indicate that gas-rich mergers are capable of triggering strong star formation episodes. The immediate

aftermath of such an event is predicted to be a largely spheroidal remnant with a blue core, widespread morphological disturbances such as tidal tails and young star clusters (e.g. Mihos & Hernquist 1994; Bekki, Shioya & Couch 2001). Indeed, the study of Yang et al. (2004) has found a striking correspondence between the predicted properties of merger remnants and the observed characteristics of blue E+A galaxies.

Numerous authors have studied E+A galaxies using a variety of indicators, which allows us to infer the characteristics of the (recent) starburst that dominates the spectra of these systems. While the age of the burst should be approximately  $\sim 1$  Gyr, simply by virtue of A-type stars being present, the mass fractions forming in the burst are inferred to be quite high. Yang et al. (2004) estimate that 50 per cent of the mass may form in the burst, allowing the E+A galaxies to fade on to the E/S0 fundamental plane in a few Gyr after the event. Norton et al. (2001), who analysed the entire Zabludoff et al. (1996) sample, estimate that the fraction of stellar mass in young (A-type) stars is typically between 30 and 80 per cent. Bressan, Poggianti & Franceschini (2001) infer a similarly high-mass fraction of 60 per cent for the sample of E+A galaxies in Poggianti, Bressan & Franceschini (2001), while Liu & Green (1996) derive mass fractions typically greater than 20 per cent (and as high as 100 per cent) for eight E+A galaxies taken from the literature [but note that Liu et al. (2007) revise the inferred mass fraction to lower values for one of their E+A galaxies – G515]. While E+As are, by definition, presently quiescent, an estimate of the SFR that *might* have characterized the recent starburst can be estimated from dusty starburst galaxies which show an E+A signature in their spectra. Poggianti & Wu (2000) estimate the SFRs in these systems to be between 50 and 300  $M_{\odot}$  per year.

While mergers and interactions might trigger star formation, the exact mechanism by which the starburst is subsequently quenched remains largely unexplained. Star formation is, of course, inherently subject to ‘negative feedback’ since the SFR depends on the mass of cold gas available. As star formation proceeds and the gas reservoir is exhausted, the rate of further star formation activity correspondingly decreases. However, the properties of E+A galaxies are generally inconsistent with such a gradual, self-modulated decline in the SFR and imply a more abrupt quenching of star formation activity.

Common sources of kinetic and thermal ‘feedback’ that might be capable of quenching star formation, e.g. by ejecting or heating the gas reservoir, include supernovae (SN), which are effective mainly in low-mass galaxies due to their shallow potential wells, and active galactic nuclei (AGN), which are thought to operate in massive galaxies where SN feedback is not energetic enough to ‘disable’ the cold gas reservoir. Goto (2006) has demonstrated that some galaxies which contain signatures of an active AGN also exhibit post-starburst signatures, indicating that a connection exists between these two phenomena. They find that the post-starburst regions are centred around the AGN, the spatial proximity implying that AGN activity could plausibly affect the region around it. Indeed, the fact that the AGN *outlives* the starburst is an indication that it may have played a role in the quenching of star formation.

In this study, we extend the existing literature on post-starburst galaxies by performing the first study of E+A systems that incorporates their ultraviolet (UV) photometry. The extreme sensitivity of the UV to young stars allows us to put strong constraints on the star formation history (SFH) of galaxies within the last  $\sim 2$  Gyr. The addition of UV photometry alleviates the age–metallicity degeneracy that commonly plagues optical studies (Kaviraj et al. 2007), allowing us to better quantify the recent SFH than can be achieved using optical data alone. Indeed, the sensitivity of the UV to young stars

has recently been exploited to demonstrate that early-type galaxies, traditionally thought to be entirely quiescent systems, exhibit *widespread* evidence for low-level recent star formation, consistent with the expectations of the standard  $\Lambda$ CDM model (Kaviraj et al. 2006a).

In this paper, we exploit the properties of the UV to accurately reconstruct the recent SFH of individual E+A galaxies. By comparison to a large library of models, we derive estimates for the ages of the recent bursts, the mass fractions formed in them and the time-scales over which they occurred. By comparing the derived time-scales to the dynamical time-scales of the galaxies, we explore the efficiency with which star formation has been quenched in these systems and study how this quenching efficiency varies as a function of galaxy properties such as mass, luminosity and stellar velocity dispersion. We use simple energetic arguments to study whether the characteristics of the quenching are consistent with feedback from SN and AGN. Finally, we study the time-scale over which E+A galaxies can evolve from their present positions in the blue cloud to the red sequence. Since E+As are, by definition, at the point of truncation of their star formation, it is possible to get a rather ‘clean’ estimate of this migration time-scale by studying the evolution in both UV and optical colours.

## 2 SAMPLE SELECTION

We use the publicly available Garching SDSS catalogue<sup>1</sup> to select E+A galaxies from the SDSS DR4. The criteria used for E+A selection follow that of Goto (2005):  $H\delta$  (EW)  $> 5.0 \text{ \AA}$  (measured in the wider window of 4082–4122  $\text{\AA}$ ),  $H\alpha$  (EW)  $> -3.0 \text{ \AA}$  and  $[O\text{II}]$  (EW)  $> -2.5 \text{ \AA}$ . Absorption lines have a positive sign in these definitions. Note that including the equivalent width of the  $H\alpha$  line makes the selection criteria stronger, because using *only* the  $[O\text{II}]$  line could result in more than 50 per cent of the selected galaxies having measurable  $H\alpha$  emission (e.g. Goto et al. 2003). In addition to the line measurements, we also use estimates of stellar mass and AGN classifications provided by the Garching SDSS catalogue. The line index measurements in this catalogue were calculated using the code of Tremonti et al. (2004), while stellar mass estimates and AGN classifications were taken from a series of comprehensive analyses of the local galaxy population observed by the SDSS (Kauffmann et al. 2003b,a; Brinchmann et al. 2004).

To ensure the accuracy of the line measurements, the sample was restricted to galaxies where the median signal-to-noise ratio of the spectrum is greater than 10. Galaxies which show evidence of an active AGN were removed, because scattered light from the AGN could contaminate the UV continuum and affect the derived parameters presented later in this analysis. Finally, the sample was restricted to galaxies in the redshift range  $0 < z < 0.2$ , since the UV filters used in the analysis (see below) trace flux bluewards of the UV continuum at higher redshifts.

This E+A sample, drawn from the SDSS DR4, was then cross-matched with publicly available UV photometry from the second data release of the Galaxy Evolution Explorer (GALEX) mission (Martin et al. 2005). GALEX provides two UV filters: the far-ultraviolet (FUV) centred at  $\sim 1530 \text{ \AA}$  and the near-ultraviolet (NUV) centred at  $\sim 2310 \text{ \AA}$ . This cross-matching produced 38 E+A galaxies which have *at least* a detection in the NUV filter, 28 of which have photometry in both the FUV and NUV filters.

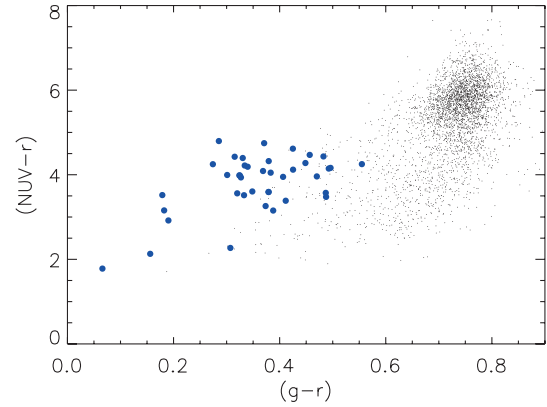


**Figure 1.** The position of our E+A galaxies (filled blue circles) in the  $(\text{NUV} - r)$  versus  $(g - r)$  colour space, compared to a sample of early-type galaxies drawn from the SDSS DR5 using the method of Kaviraj et al. (2006b) and cross-matched with GALEX. The E+A population inhabits the blue cloud and is well separated from the early-type galaxies which define the bulk of the red sequence. Note that the colours are in the observed frame, i.e. they are shown without applying  $K$ -corrections.

Fig. 1 shows the position of our E+A galaxies (filled blue circles) in the  $(\text{NUV} - r)$  versus  $(g - r)$  colour space, compared to a sample of early-type galaxies drawn from the SDSS DR5 using the method of Kaviraj et al. (2006b) and cross-matched with the GALEX second data release. It is apparent that the E+A population is well separated from the early-type population which defines the bulk of the red sequence. Comparison to fig. 1 in Yi et al. (2005) indicates that E+A galaxies inhabit the blue cloud.

Since previous studies have indicated that E+A galaxies are potential progenitors of early-type galaxies, we check the morphologies of the E+A galaxies in our sample using the SDSS *fracDev* parameter. The SDSS pipeline fits both deVaucouleur’ s and exponential surface brightness profiles to galaxy images (in each filter) and creates a composite *best-fitting* profile using a linear combination of the two fits. The *fracDev* parameter is the weight of the deVaucouleur’ s profile in this composite fit. Thus, galaxies with large values of *fracDev* can be considered to have spheroidal morphology. We find that all but six of the galaxies studied in this sample have *fracDev*  $> 0.8$  in the  $r$  band, which indicates that the majority of E+A galaxies in this sample are indeed spheroidal systems. It is worth noting that all six galaxies which have *fracDev*  $< 0.8$  are low-mass systems ( $M < 10^{10} M_{\odot}$ ) and their non-deVaucouleur’ s morphologies are consistent with the fact that dwarf ellipticals typically show exponential surface brightness profiles.

## 3 PARAMETER ESTIMATION

We estimate parameters governing the SFH of each E+A galaxy by comparing their (FUV, NUV,  $u$ ,  $g$ ,  $r$ ,  $i$ ,  $z$ ) photometry to a library of synthetic photometry generated using a large collection of model SFHs. Each SFH is constructed by assuming that an instantaneous burst of star formation at high redshift ( $z \sim 3$ ) is followed by a second burst which is modelled as an exponential.

Fig. 2 shows a schematic representation of the model SFHs. The free parameters in this analysis are the age ( $t_2$ ), mass fraction ( $f_2$ ) and time-scale ( $\tau_2$ ) of the second burst.  $t_2$  is allowed to vary from 0.05 Gyr to the look-back time corresponding to  $z = 3$  in the rest frame of each E+A galaxy.  $f_2$  varies between 0 and 1 and  $\tau_2$  is allowed to vary from 0.01 to 4 Gyr. Since our focus is purely on E+A

<sup>1</sup> <http://www.mpa-garching.mpg.de/SDSS/DR4/>

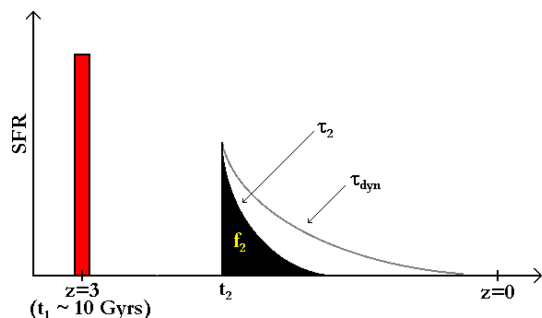


**Figure 2.** Model SFHs (see Section 2) are constructed by assuming that an instantaneous burst of star formation at high redshift ( $z \sim 3$ ) is followed by a second burst, modelled as an exponential. The free parameters are the age ( $t_2$ ), mass fraction ( $f_2$ ) and time-scale ( $\tau_2$ ) of the second burst.  $t_2$  is allowed to vary from 0.05 Gyr to the look-back time corresponding to  $z = 3$  in the rest frame of each E+A galaxy.  $f_2$  varies between 0 and 1 and  $\tau_2$  is allowed to vary from 0.01 to 4 Gyr.  $\tau_{\text{dyn}}$  indicates the dynamical time-scale of the galaxy. More catastrophic quenching leads to smaller values of the ratio  $\tau_2/\tau_{\text{dyn}}$ , which is used in Section 5 to parametrize the *efficiency* with which quenching occurs in the E+A galaxies studied here.

galaxies, we must, by definition, exclude models which contain ongoing star formation. Therefore, we only keep models where the intensity of star formation in the second burst at present day is less than 5 per cent of the intensity when the burst started.<sup>2</sup> Changing this threshold to less than 5 per cent leaves our results unchanged. Note that excluding models that have ongoing star formation reduces the allowed parameter space of model SFHs, resulting in much tighter constraints on the parameters, in particular, the time-scale of star formation  $\tau_2$ .

The motivation for an instantaneous burst at high redshift stems from the fact that, as potential progenitors of spheroidal galaxies, one expects a substantial fraction of stellar mass to have formed at high redshift in these galaxies (e.g. Bower, Lucey & Ellis 1992; Kaviraj et al. 2006b). Furthermore, since the UV is insensitive to stellar populations older than  $\sim 2$  Gyr coupled with the fact that optical colour evolution virtually stops after 5–6 Gyr (e.g. Yi 2003), resolving this old burst does not affect the UV and optical colours of the model.

The UV flux in each model is completely dominated by the second burst of star formation. Even though our expectations, on the basis of the properties of E+A galaxies (and previous studies of E+A systems), are that  $t_2 \sim 1$  Gyr and  $f_2$  is high, our model library does not put a prior on these parameters – vigorous starbursts at recent epochs are allowed, as is slowly declining star formation from intermediate redshifts. In essence, the comparison between the synthetic library and observed photometry is allowed to ‘choose’ the optimum SFH that satisfies the photometry of each E+A galaxy.

To build the library of synthetic photometry, each model SFH is combined with a single metallicity in the range 0.1 to  $2.5 Z_{\odot}$  and a value of dust extinction parametrized by  $E(B - V)$  in the range 0 to 0.5. Photometric predictions are generated by combining each model SFH with the chosen metallicity and  $E(B - V)$  values and convolving with the stellar models of Yi (2003) through the GALEX, FUV, NUV and SDSS  $u, g, r, i, z$  filters. This procedure yields a synthetic library of 1.5 million models.

Since our E+A galaxies are observed at a range of redshifts, equivalent libraries are constructed at redshift intervals of  $\delta z = 0.01$ .

<sup>2</sup> This implies that models with small values of  $t_2/\tau_2$  are excluded.

A fine redshift grid is essential in such a low-redshift study because a small change in redshift produces a relatively large change in look-back time over which the UV flux can change substantially, inducing ‘K-correction-like’ errors into the analysis.

The free parameters ( $t_2, f_2$  and  $\tau_2$ ) are estimated by comparing each observed galaxy to every model in the synthetic library, with the likelihood of each model ( $\exp - \chi^2/2$ ) calculated using the value of  $\chi^2$  computed in the standard way. From the joint probability distribution, each parameter is marginalized to extract its one-dimensional probability density function (PDF). We take the median of this PDF as the best estimate of the parameter in question and the 16 and 84 percentile values as the ‘one-sigma’ uncertainties on this estimate. The cosmological parameters used in this study assume a  $\Lambda$ CDM model:  $h = 0.7, \Omega_m = 0.3$  and  $\Omega_{\Lambda} = 0.7$ .

Note that there are 10 galaxies in our sample which do not have FUV detections. The parameter estimation on these galaxies is carried out using only the NUV,  $u, g, r, i$  and  $z$ -band filters. We do not use the FUV detection limit as an upper limit to the FUV flux.

#### 4 CHARACTERISTICS OF THE RECENT BURST: AGES, MASS FRACTIONS AND TIME-SCALES

We begin by presenting estimates for the basic parameters ( $t_2, f_2$  and  $\tau_2$ ) that describe the burst of star formation that immediately precedes the quenching in our E+A galaxies. The top panel of Fig. 3

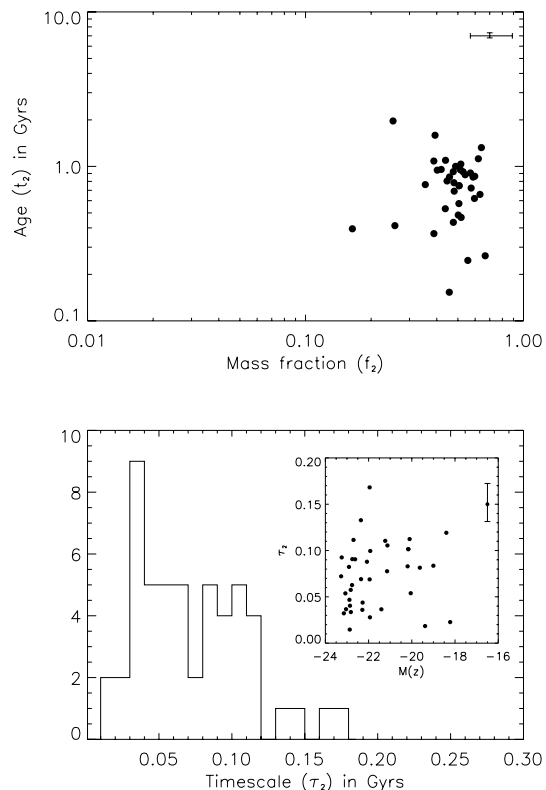


**Figure 3.** Top panel: ages and mass fractions of the burst that creates the E+A galaxies in our sample. Burst ages are typically within a Gyr, as one expects from the lifetimes of A-type stars which contribute significantly to E+A spectra. We recover large mass fractions, typically higher than 10 per cent and possibly as high as 70 per cent, consistent with previous studies. Bottom panel: effective time-scales of the starbursts in E+A galaxies. The time-scales are typically short – between 0.01 and 0.2 Gyr – implying that the SFRs during the burst phase are high (see text in Section 4 and Fig. 4).

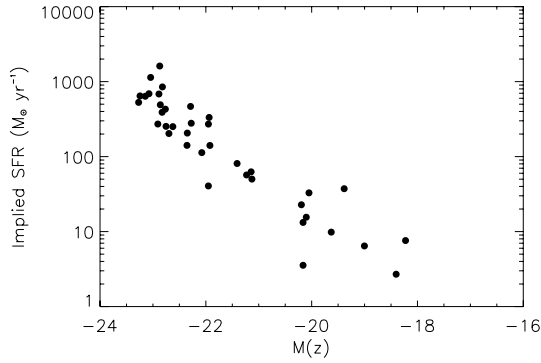


**Figure 4.** Implied SFRs during the burst phase in E+A galaxies. The implied SFR is estimated by dividing the stellar mass formed by the time-scale of the burst. Note that, since the burst lasts longer than one time-scale, the SFRs are overestimated. However, the estimates probably give a reasonable indication of the SFR during the most intense period of the starburst.

shows the ages and mass fractions of the recent burst in each E+A galaxy. The burst ages are typically within 2 Gyr, as one expects from the lifetimes of A-type stars which contribute significantly to E+A spectra. In agreement with previous studies, we derive large mass fractions, which are typically higher than 10 per cent and possibly as high as 70 per cent in some galaxies. The bottom panel shows the time-scales over which the bursts take place. The time-scales are typically short – between 0.01 and 0.2 Gyr – implying that the SFRs during the burst phase are extremely high.

We can estimate this ‘implied’ SFR by dividing the stellar mass formed by the time-scale of the burst (Fig. 4). We note that, since the burst lasts longer than one time-scale, the SFRs are overestimated. However, the estimates probably give a reasonable indication of the SFR during the most intense period of the starburst and we find a tight correlation between the mass of the E+A galaxy and the implied SFR (see bottom panel of Fig. 3). While low-luminosity [ $M(z) > -20$ ] E+As have implied SFRs of less than  $50 M_{\odot} \text{ yr}^{-1}$ , E+A systems at the high-luminosity end [ $M(z) < -22$ ] exhibit SFRs of greater than 300, and as high as  $2000 M_{\odot} \text{ yr}^{-1}$ .

The high SFRs inevitably lead to comparisons with luminous and ultra-luminous infrared galaxies (LIRGs/ULIRGs), whose high infrared luminosities ( $L_{\text{IR}} > 10^{11} L_{\odot}$ ) imply massive ongoing starbursts (e.g. Sanders & Mirabel 1996). SFRs in LIRGs ( $10^{11} L_{\odot} < L_{\text{IR}} < 10^{12} L_{\odot}$ ) typically exceed a few tens of solar masses per year, while in ULIRGs ( $L_{\text{IR}} > 10^{12} L_{\odot}$ ) the SFRs can be as high as hundreds of solar masses per year (e.g. Kennicutt 1998). Wang et al. (2006), who have performed a study of LIRGs in the nearby Universe ( $z \sim 0.1$ ), find SFRs of between 10 and  $100 M_{\odot} \text{ yr}^{-1}$  for their sample of galaxies (see their fig. 5). Noting that our SFRs are overestimated, and could be a few factors too high, we suggest that LIRGs at low redshift *could* transform into massive E+A galaxies. However, we note that the robustness of such a conclusion depends on performing an identical parameter estimation on LIRGs at low redshift and by considering whether other factors, such as the local environments of E+A galaxies, correspond closely to those of LIRGs.

## 5 THE EFFICIENCY OF QUENCHING AS A FUNCTION OF GALAXY MASS

One of the primary goals of this paper is to study the characteristics of the quenching that truncates the burst and determine the possible mechanisms by which this quenching could occur. A key parameter

in this analysis is the *efficiency* with which the star formation is quenched. We study this ‘quenching efficiency’ by comparing the effective time-scale of the burst,  $\tau_2$ , to the dynamical time-scale<sup>3</sup> of the galaxy,  $\tau_{\text{dyn}}$ , which is defined as

$$\tau_{\text{dyn}} = \left( \frac{2R^3}{GM} \right)^{1/2}, \quad (1)$$

and describes the ‘natural’ time-scale over which processes such as star formation would take place if left *unhindered*.<sup>4</sup> Note that, in the calculations that follow, we have used the stellar mass of the galaxy as the value of  $M$ . We parametrize the quenching efficiency by constructing the time-scale ratio

$$r_{\tau} = \tau_2 / \tau_{\text{dyn}}. \quad (2)$$

More efficient quenching reduces  $\tau_2$  and therefore produces a lower value for  $r_{\tau}$ . The time-scale ratio is, therefore, *inversely correlated* with quenching efficiency – more catastrophic quenching results in lower values of  $r_{\tau}$ .

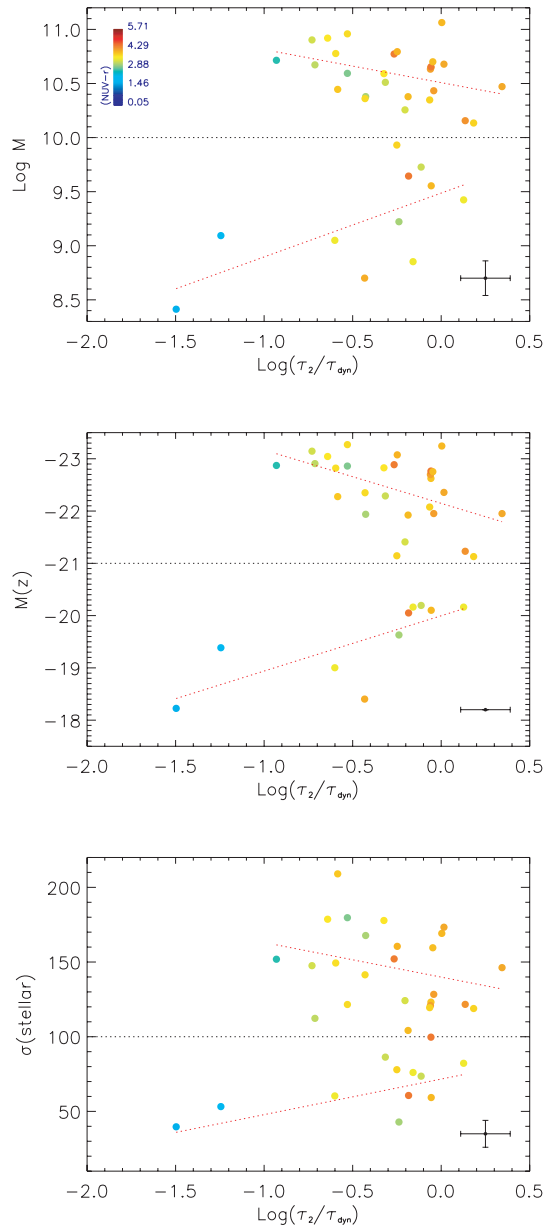
In Fig. 5, we plot  $r_{\tau}$  against three independent indicators of galaxy mass/luminosity. The galaxies are colour-coded using their (NUV –  $r$ ) colour. The plot of  $r_{\tau}$  versus galaxy mass (top panel) reveals a striking difference in the behaviour of  $r_{\tau}$  with increasing galaxy mass. We find that, below a mass of  $10^{10} M_{\odot}$ , the quenching efficiency decreases with increasing galaxy mass. However, when the galaxy mass is greater than  $\sim 10^{10} M_{\odot}$ , this trend is reversed and the quenching efficiency then correlates positively with the galaxy mass. We check this behaviour with both  $M(z)$  and stellar velocity dispersion. We find that the correlation of  $r_{\tau}$  with galaxy mass and, in particular, its apparent reversal is present in all the separate indicators of galaxy mass/luminosity. While a strong trend is apparent with stellar mass ( $M$ ) and  $z$ -band luminosity, the trend is weaker in the stellar velocity dispersion ( $\sigma$ ), most probably driven by bigger uncertainties in the  $\sigma$  measurement (as suggested by the larger scatter in this plot). A plausible source of uncertainty is the fact that the E+A galaxies are unresolved (indeed a significant fraction look disturbed in the SDSS images), implying that  $\sigma$  does not yet trace the virial mass of the galaxy. An additional source of uncertainty is the presence of a substantial young stellar population. The presence of young sub-components could create a bias towards lower values of  $\sigma$ , with the magnitude of the bias driven by the mass fraction and age of the young stars and on the exact size of the physical aperture subtended by the SDSS spectra in each galaxy. We therefore suggest that the correlation between  $r_{\tau}$  and  $\sigma$  should be treated with caution considering the caveats we have presented above.

Fig. 5 shows that the reversal in the  $r_{\tau}$  correlation occurs at  $M \sim 10^{10} M_{\odot}$ ,  $M(z) \sim -21$  and  $\sigma \sim 100 \text{ km s}^{-1}$  when  $r_{\tau}$  is plotted against mass, absolute  $z$ -band luminosity and stellar velocity dispersion, respectively. The dichotomy in the trend of  $r_{\tau}$  against galaxy mass indicates that the principal quenching mechanisms for galaxies above and below the mass threshold of  $10^{10} M_{\odot}$  behave very differently. In particular, the mechanism that operates in the regime  $M < 10^{10} M_{\odot}$  becomes *weaker* as the galaxy mass increases while the mechanism that operates in the regime  $M > 10^{10} M_{\odot}$  becomes *stronger* as the galaxy mass increases.

The mass threshold ( $10^{10} M_{\odot}$ ) at which the  $r_{\tau}$  versus  $M$  trend reverses is particularly interesting because it is in excellent agreement

<sup>3</sup> Using  $s = \frac{1}{2}at^2$  from the equations of motion, the dynamical time-scale follows by setting  $a = g = (GM/R^2)$  and  $s = R$ .

<sup>4</sup> Note that we use the radius that contains 90 per cent of the Petrosian flux in the  $i$  band as the value of  $R$ .



**Figure 5.** The time-scale ratio,  $r_\tau = \tau_z/\tau_{\text{dyn}}$ , plotted against galaxy mass (top), absolute  $z$ -band luminosity (middle) and stellar velocity dispersion (bottom). Note that the red dotted lines indicate standard least-squares fits to the data. The fits are performed separately for the massive ( $M > 10^{10} M_\odot$ ) and low-mass ( $M < 10^{10} M_\odot$ ) E+A galaxies in each panel.

with the mass above which AGN become significantly more abundant in galaxies in the nearby Universe (Kauffmann et al. 2003b). Given this result, the reversal at  $M \sim 10^{10} M_\odot$  can be explained, at least qualitatively, in terms of SN and AGN being the principal quenching sources above and below this mass threshold. In the absence of AGN, the primary source of negative feedback is SN. As galaxies become more massive and the depth of the potential well increases, SN find it increasingly more difficult to eject gas from the system. This results in the quenching becoming less efficient at higher galaxy masses, exactly as we observe in Fig. 5.

However, once AGN begin to appear (above  $M \sim 10^{10} M_\odot$ ), they become the dominant source of negative feedback. For a  $10^{11} M_\odot$  galaxy, the energy input from a population of (Type II) SN formed

as a result of a starburst that creates half the stellar mass of the galaxy is  $\sim 3 \times 10^{57}$  erg,<sup>5</sup> while the energy output from a central AGN, emitting at the Eddington limit<sup>6</sup> over a time-scale of 0.1 Gyr, is  $\sim 3 \times 10^{58}$  erg.<sup>7</sup> In terms of energy input, the AGN dominates and it is reasonable to assume that it dictates the mechanics of the quenching. Note that we did not consider Type Ia SN in this calculation because the derived time-scales (see Fig. 3) are considerably shorter than 1 Gyr, which is the typical time delay between the onset of star formation and the appearance of Type Ia SN.

Given that the mass of the BH ( $M_{\text{BH}}$ ) scales with the central velocity dispersion  $\sigma$  as  $M_{\text{BH}} \sim \sigma^\beta$  (Ferrarese & Merritt 2000; Gebhardt et al. 2000), where  $\beta$  varies in the range 4–5, and assuming the energy outputted by the AGN scales with  $M_{\text{BH}}$  (cf. the Eddington luminosity  $L_{\text{edd}} \propto M_{\text{BH}}$ ), we expect AGN feedback to become more effective, and thus the quenching efficiency to increase, as galaxy mass increases. Again, this is indeed what we observe in Fig. 5. We briefly note that, by definition, our sample does not contain galaxies that show signs of *current* AGN activity, implying that the AGN has shut itself off in the process of providing feedback. If, as we argue below, mechanical feedback from the AGN depletes the gas reservoir, then this process also removes the AGN’s own fuel source. Thus, it is plausible that the feedback process *simultaneously* quenches both star formation and AGN activity.

It is worth noting that a similar dichotomy in the primary feedback mechanism has been inferred by Shankar et al. (2006), from a study of the stellar and baryonic mass functions of galaxies, extracted using the mass-to-light ratios of stars and gas derived from galaxy kinematics.

## 6 THE EXPECTED DEPENDENCE OF THE QUENCHING EFFICIENCY ON GALAXY MASS

We now use simple energetic arguments to derive the expected relationship between the time-scale ratio  $r_\tau$  and galaxy mass in the two cases where the quenching is due to SN and AGN, respectively.

We make the assumption that quenching takes place due to the ejection of available gas from the potential well. The energy required for quenching,  $E_q$ , is given by

$$E_q = \frac{1}{2} m_g v_{\text{esc}}^2, \quad (3)$$

where  $m_g$  is the mass of gas to be ejected and  $v_{\text{esc}}^2$  is the escape velocity. Since

$$v_{\text{esc}}^2 = \left( \frac{2GM}{R} \right), \quad (4)$$

this implies that

$$E_q \propto m_g \frac{M}{R}, \quad (5)$$

<sup>5</sup> The energy injected by a population of SN is given by  $\eta_{\text{SN}} \varepsilon_{\text{SN}} \Delta M$ , where  $\eta_{\text{SN}} (\sim 5 \times 10^{-3} M_\odot^{-1})$  is the number of SN per unit stellar mass and  $\varepsilon_{\text{SN}} (\sim 10^{51}$  erg) is the energy supplied by each supernova. The fraction of that energy that couples mechanically to the material in the interstellar medium (ISM) is approximately given by  $\sigma/20000 \text{ km s}^{-1}$ , where  $\sigma$  is the velocity dispersion and  $20000 \text{ km s}^{-1}$  is the velocity of the SN ejecta. For a  $M \sim 10^{11} M_\odot$  galaxy,  $\sigma \sim 200 \text{ km s}^{-1}$ .

<sup>6</sup> The Eddington luminosity for a mass  $M$  is  $\sim 1.3 \times 10^{38} M/M_\odot$  erg per second.

<sup>7</sup> A  $M \sim 10^{11} M_\odot$  typically hosts a  $M \sim 10^8 M_\odot$  black hole (BH), since  $(M_{\text{BH}}/M_{\text{bulge}}) \sim 10^{-3}$  (Häring & Rix 2004). The Eddington luminosity of such a BH is  $\sim 10^{46} \text{ erg s}^{-1}$ , of which a fraction  $\sigma/c \text{ km s}^{-1}$  couples mechanically to the material in the ISM.  $\sigma$  is the velocity dispersion of the galaxy and  $c$  is the speed of light.

or, equivalently, in terms of parameters derived in this analysis that

$$E_q \propto m_g \left( \frac{M}{\tau_{\text{dyn}}} \right)^{2/3} \propto m_g \left( \frac{Mr_\tau}{\tau_2} \right)^{2/3}. \quad (6)$$

The relationships in equation (6) use substitutions from equations (1) and (2). Equation (6) describes the dependence of the energy required for quenching on the time-scale ratio  $r_\tau$ , the burst time-scale  $\tau_2$  and galaxy mass  $M$ .

We now make the simplifying assumption that the mass of gas ( $m_g$ ) required to be ejected for quenching is approximately constant in all galaxies. This is consistent with the downsizing phenomenon (e.g. Cowie et al. 1996), whereby smaller galaxies exhibit higher SFRs than their massive counterparts at lower redshifts. Given the apparent universality of the Schmidt–Kennicutt law for (quiescent) star formation (Kennicutt 1998), downsizing implies that smaller galaxies tend to be more gas-rich than larger ones, justifying the empirical assumption that their *absolute* neutral gas reservoirs may have similar sizes. Cold gas fractions in low-redshift LIRGs (see fig. 5 in Wang et al. 2006), which are potential progenitors of E+A galaxies (Section 4), indeed show a declining trend with galaxy mass. Across the mass range  $10^{10.5}$ – $10^{11.5} M_\odot$ , the gas fractions increase from less than 5 per cent to greater than 25 per cent, suggesting that the cold gas reservoirs in these galaxies are similar in size and our assumption of constant  $m_g$  is a reasonable one. A small spread in the real values of  $m_g$  will induce a scatter in the trends derived in Sections 6.1 and 6.2, without perturbing the correlations between the variables. With this assumption, equation (6) becomes

$$E_q \propto \left( \frac{M}{\tau_{\text{dyn}}} \right)^{2/3} \propto \left( \frac{Mr_\tau}{\tau_2} \right)^{2/3}. \quad (7)$$

We should also note that the assumption that quenching occurs through the mechanical ejection of gas may imply that E+A galaxies should be relatively gas-poor, although the gas could simply be dispersed away from the central regions of the potential well where star formation would normally take place. Two studies of the H I content of E+A galaxies have been conducted so far. Chang et al. (2001) observed five E+A galaxies from the Zabludoff et al. (1996) sample and detected only one with an H I mass of  $\sim 3.4 \times 10^9 M_\odot$ . Similarly, Buyle et al. (2006) detected similar amounts ( $> 10^9 M_\odot$ ) of H I in three out of six E+A galaxies they observed in H I. While, it might be useful to compare the gas masses estimated by e.g. Buyle et al. (2006) for E+A galaxies to those estimated for LIRGs (as potential progenitors) by Wang et al. (2006), the mass ranges traced by these two studies are quite different. Buyle et al. (2006) trace galaxies with  $M \lesssim 10^{10.7} M_\odot$ ,<sup>8</sup> while Wang et al. (2006) study galaxies with  $M \gtrsim 10^{10.6} M_\odot$ . The small overlap region around  $10^{10.7} M_\odot$  indicates that the H I fraction<sup>9</sup> in the LIRGs may be higher by a factor of 3. We note, however, that due to the inadequate overlap between the two samples, this result is not very robust. However, given the apparent lack of H I in the majority of E+As observed by Chang et al. (2001) and the smaller gas fractions found in Buyle et al. (2006) compared to nearby LIRGs (which have comparable

<sup>8</sup> The masses of the Buyle et al. (2006) galaxies have been estimated by converting the values of  $M(B)$  given in their table 1 to  $M(z)$ , which are then converted to masses using the  $M$  versus  $M(z)$  relation for the E+A galaxies in our sample.

<sup>9</sup> Note that we have converted the  $H_2$  mass [which is the quantity estimated by Wang et al. (2006)] to an H I mass, using the average  $H_2/\text{H I}$  ratio for late-type galaxies ( $\sim 0.6$ ) given by (Fukugita, Hogan & Peebles 1998, see their table 1)

SFRs to our E+A galaxies), the assumption of quenching through the mechanical ejection of gas seems reasonable.

### 6.1 Quenching by SN

The energy injected by SN into the ISM is proportional to the amount of stellar mass produced in the burst so that

$$E^{\text{SN}} = \eta_{\text{SN}} \varepsilon_{\text{SN}} \Delta M, \quad (8)$$

where  $\eta_{\text{SN}}$  is the number of SN per unit stellar mass,  $\varepsilon_{\text{SN}}$  is the energy supplied by each supernova and  $\Delta M$  is the amount of stellar mass formed. Hence,

$$E^{\text{SN}} \propto f_2 M, \quad (9)$$

since  $\Delta M = f_2 M$ . Combining equations (7) and (9) gives

$$r_\tau^2 \propto \tau_2^2 f_2^3 M, \quad (10)$$

so that

$$\log(\tau_2^2 f_2^3 M) = 2 \log(r_\tau) + k. \quad (11)$$

As we would naively expect from SN-driven feedback,  $r_\tau$  correlates with the galaxy mass ( $M$ ). Since  $r_\tau$  is inversely correlated to the quenching efficiency, this implies that, as galaxy mass increases, the quenching efficiency decreases in the SN feedback scenario. Defining  $Q_{\text{SN}} = \tau_2^2 f_2^3 M$ , we have

$$\log(Q_{\text{SN}}) = 2 \log(r_\tau) + k, \quad (12)$$

where  $k$  absorbs the constants in the proportionality relations used to derive equation (12). A plot of  $\log(Q_{\text{SN}})$  against  $\log(r_\tau)$  should therefore show a gradient of 2, if the systems being considered are indeed quenched *purely* by SN.

In Fig. 6, we plot  $r_\tau$  versus  $Q_{\text{SN}}$  for both low-mass ( $M < 10^{10} M_\odot$ ; black) and massive ( $M > 10^{10} M_\odot$ ; red) galaxies. The solid lines indicate standard least-squares fits to the data. We find that, while low-mass galaxies show a gradient of  $1.98 \pm 0.18$  (and are therefore consistent with the expected gradient of 2), the best-fitting relation for the massive galaxies is too shallow ( $0.56 \pm 0.06$ ) and does not satisfy the predictions. We conclude, therefore, that low-mass galaxies show good consistency with being quenched *purely* by SN feedback while massive galaxies are essentially inconsistent with such a picture.

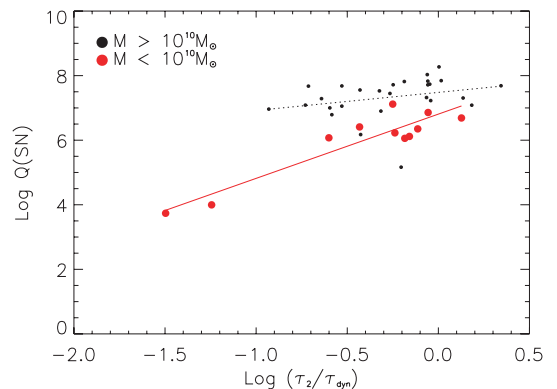


**Figure 6.**  $r_\tau$  versus  $Q_{\text{SN}}$  for galaxies with  $M > 10^{10} M_\odot$  (black) and  $M < 10^{10} M_\odot$  (red). The solid lines indicate standard least-squares fits to the data.

## 6.2 Quenching by AGN

The energy injected by an AGN ( $E^{\text{AGN}}$ ) is driven by its luminosity ( $L$ ) so that

$$E^{\text{AGN}} \propto L \tau_2. \quad (13)$$

Rewriting equation (13) in terms of the Eddington luminosity ( $L_{\text{edd}}$ ), we have

$$E^{\text{AGN}} \propto \mu L_{\text{edd}} \tau_2, \quad (14)$$

where  $\mu = L/L_{\text{edd}}$  is the Eddington ratio.  $L_{\text{edd}}$  is proportional to the mass of the central BH ( $M_{\text{BH}}$ ), which in turn has been shown to scale with the central velocity dispersion ( $\sigma$ ) of the galaxy as  $M_{\text{BH}} = \sigma^\beta$ . Estimates of  $\beta$  vary in the range 4–5, with Gebhardt et al. (2000) reporting  $\beta = 3.75 \pm 0.3$ , while Ferrarese & Merritt (2000) reporting  $\beta = 4.8 \pm 0.5$ . For simplicity, we begin by assuming that  $\mu$  is constant across our entire sample of AGN. Then,

$$E^{\text{AGN}} \propto \sigma^\beta \tau_2. \quad (15)$$

Since, the virial theorem<sup>10</sup> implies that  $\sigma^2 \sim M/R$ , we rewrite this as

$$E^{\text{AGN}} \propto \frac{M^{\beta/3} r_\tau^{\beta/3}}{\tau_2^{\beta/3}} \tau_2, \quad (16)$$

where we have used equations (1) and (2) to eliminate  $R$  and explicitly introduce the time-scale ratio  $r_\tau$ . Equating equations (7) and (16) then gives

$$r_\tau^{(2-\beta)} \propto M^{(\beta-2)} \tau_2^{(5-\beta)}. \quad (17)$$

Using  $\beta \sim 5$  from Ferrarese & Merritt (2000) then implies that

$$M \propto r_\tau^{-1} \quad (18)$$

or that

$$\log M = -\log(r_\tau) + k, \quad (19)$$

where  $k$  absorbs the constants in the proportionality relations used to derive equation (18). We find that a plot of  $\log M$  against  $\log r_\tau$  should show a gradient of  $-1$ , if the systems being considered are indeed quenched by AGN which have similar Eddington ratios, regardless of their size. Equation (18) explicitly predicts that, for galaxies which are quenched by AGN alone, the quenching efficiency (which is inversely correlated to  $r_\tau$ ) increases as the mass of the galaxy increases.

We now refer back to Fig. 5 (top panel), where we have plotted the dependence of  $r_\tau$  on galaxy mass for both massive and low-mass galaxies. It is clear that low-mass galaxies are inconsistent with the energetics of AGN-driven quenching, since for these systems  $r_\tau$  correlates positively with galaxy mass. Massive galaxies, on the other hand, do show an inverse correlation with  $r_\tau$ . However, the observed gradient in the correlation in Fig. 5 is  $-0.36 \pm 0.11$ , shallower than the predicted gradient of  $-1$ .

This discrepancy arises due to our assumption, in equation (13), that the Eddington ratio during the burst phase ( $\mu$ ) does not change as a function of host galaxy mass. Clearly, if  $\mu$  decreases, then the rate of energy output ( $L$ ) also decreases and a longer time-scale ( $\tau_2$ ) is required to inject the same amount of energy. This, in turn, implies a larger value of  $r_\tau$ .

<sup>10</sup> The virial theorem states that for a system with kinetic energy  $K$  and potential energy  $U$ ,  $2K + U = 0$ . For a mass distribution of mass  $M$  and radius  $R$ ,  $K \sim \frac{1}{2} M \sigma^2$  and  $U \sim \frac{GM}{R}$ , which implies that  $\sigma^2 \sim M/R$ .

We now refine our previous analysis by allowing the Eddington ratio to vary as a function of mass so that

$$\mu = M^\gamma. \quad (20)$$

With this dependence on  $M$ , equation (16) becomes

$$E^{\text{AGN}} \propto \frac{M^{\beta/3} r_\tau^{\beta/3}}{\tau_2^{\beta/3}} \tau_2 M^\gamma, \quad (21)$$

so that

$$r_\tau^{(2-\beta)} \propto M^{(3\gamma+\beta-2)} \tau_2^{(5-\beta)}. \quad (22)$$

Using  $\beta \sim 5$  as before then gives

$$M \propto r_\tau^{-1/(1+\gamma)}. \quad (23)$$

Comparison with the observed gradient of  $-0.36 \pm 0.11$  implies that  $1 < \gamma < 3$ . We find, therefore, that the observed gradient in the  $\log M$  versus  $\log r_\tau$  correlation can be reproduced if the Eddington ratio of the E+A galaxies is assumed to vary with  $M$ . Since the E+A masses are spread over an order of magnitude, this implies that the Eddington ratios of the smallest AGN (with host galaxy masses  $M \sim 10^{10} M_\odot$ ) in this sample of galaxies are *at least* one-tenth of those for their most massive counterparts in this sample (if  $\gamma \sim 1$ ).

Finally, it is instructive to calculate if a variable Eddington ratio (with  $1 < \gamma < 3$ ) might indeed be expected from simple arguments. The luminosity ( $L$ ) of an AGN is proportional to the mass accretion rate ( $\dot{M}$ ). Spherical, Bondi–Hoyle accretion (Bondi & Hoyle 1944) implies that  $\dot{M}$  is proportional to the square of the mass of the central BH, i.e.

$$L \propto \dot{M} \propto M_{\text{BH}}^2. \quad (24)$$

Since the Eddington luminosity ( $L_{\text{edd}}$ ) is proportional to  $M_{\text{BH}}$ , we have

$$\frac{L}{L_{\text{edd}}} \propto M_{\text{BH}}. \quad (25)$$

The BH mass is typically a constant fraction of the mass of the bulge (e.g. Häring & Rix 2004) with

$$\frac{M_{\text{BH}}}{M_{\text{bulge}}} \sim 10^{-3}, \quad (26)$$

which implies that

$$\mu = \frac{L}{L_{\text{edd}}} \propto M, \quad (27)$$

where we have assumed that the E+A galaxies in our sample are bulge-dominated. Such a scenario implies that the expected value of  $\gamma$  in the analysis presented above is  $\sim 1$ , which is consistent with the derived range ( $1 < \gamma < 3$ ).

Assuming a more general dependence of  $\dot{M}$  on  $M_{\text{BH}}$  ( $\dot{M} \propto M_{\text{BH}}^\lambda$ ) would imply that

$$\frac{L}{L_{\text{edd}}} \propto M^{\lambda-1}. \quad (28)$$

$\lambda - 1$  is equal to  $\gamma$  in equation (20) and the Eddington ratio increases with host galaxy mass (as is required to satisfy the shallower gradient in the  $\log M$  versus  $\log r_\tau$  relation) if  $\lambda \gtrsim 2$ . For Bondi–Hoyle accretion  $\lambda \sim 2$ .

## 7 MIGRATION TIME TO THE RED SEQUENCE

Galaxy colours show a pronounced bi-modality over a large range in redshift. This dichotomy in the colours, combined with the build-up of the red sequence over time (e.g. Bell et al. 2004), indicates that

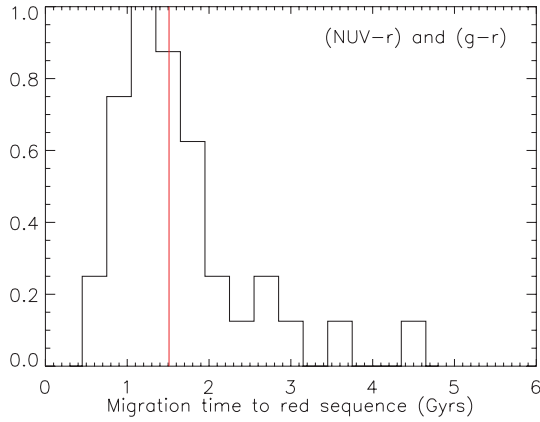


**Figure 7.** Histogram showing the migration time of E+A galaxies from the blue cloud to the red sequence in both the UV and optical colours. The median migration time (indicated by the solid red line) is  $\sim 1.5$  Gyr. The y-axis shows the frequency normalized to 1.

a central feature of the evolution of the galaxy population is the net migration of galaxies from the blue cloud on to the red sequence. Therefore, in the context of understanding the macroscopic evolution of galaxies, it is useful to have an estimate of the typical time it takes to complete this migration.

Given the very recent truncation of star formation in these systems, E+A galaxies are just about to begin this migration process. Assuming there is negligible star formation during this phase, we can use our derived SFHs to estimate the time it takes for galaxies to move from the blue cloud to the red sequence in *both* the UV and optical colours. The use of E+A galaxies and the fact that we study the migration in *both* the UV and the optical spectrum make the derived migration times quite robust. Note that we define the red sequence as the part of the  $(NUV - r)$  versus  $(g - r)$  colour space that hosts the bulk of the *red* early-type population. Comparison to Fig. 1 indicates that the red sequence lies redward of  $(NUV - r) \sim 5.5$  and  $(g - r) \sim 0.7$ .

We estimate the migration times by ‘ageing’ the *best-fitting* model SFHs of each E+A galaxy, keeping secondary parameters such as metallicity and  $E(B - V)$  constant. We find that the migration times vary between 1 and 5 Gyr (Fig. 7). Most galaxies complete their migration within 2 Gyr and the median migration time of galaxies in this sample (shown using the solid red line) is  $\sim 1.5$  Gyr. Finally, in Fig. 8 we show the migration tracks of the E+A sample in the  $(NUV - r)$  versus  $(g - r)$  colour space (top panel) and the  $(NUV - r)$  versus  $M(z)$  colour–magnitude space (bottom panel). Ages along the track are shown colour-coded.

## 8 CONCLUSIONS

We have presented the first study of nearby E+A galaxies which incorporates their UV photometry. By exploiting the sensitivity of the UV to young stars, we have accurately reconstructed the recent star formation histories of 38 E+A galaxies in the nearby Universe ( $0 < z < 0.2$ ) by combing optical ( $u, g, r, i, z$ ) and UV data from the SDSS and GALEX surveys, respectively.

We find that the burst of star formation that dominates the post-starburst signatures in these galaxies typically takes place within a Gyr, which is consistent with the presence of A-type stars in these systems. The stellar mass fractions formed in this burst are typically high, ranging from 20 to 60 per cent of the mass of the E+A remnant.

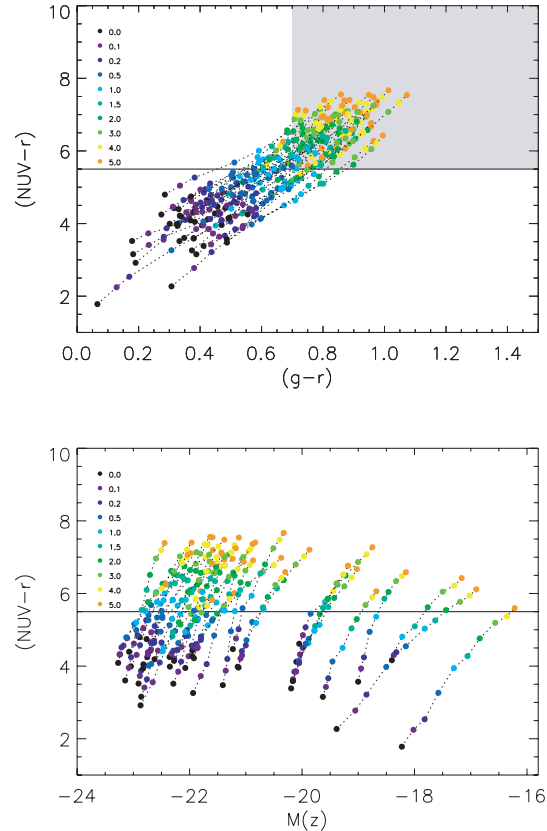


**Figure 8.** Migration tracks of E+A galaxies in the  $(NUV - r)$  versus  $(g - r)$  colour space (top panel) and the  $(NUV - r)$  versus  $M(z)$  colour–magnitude space (bottom panel). Ages (in Gyr) along the track are shown colour-coded.

The time-scale over which this star formation takes place is short, ranging between 0.01 and 0.2 Gyr. The combination of short time-scales and high mass fractions implies high SFRs during the burst. We find a tight, positive correlation between the mass of the E+A galaxy and the implied SFR. While low-luminosity [ $M(z) > -20$ ] E+As have implied SFRs of less than  $50 M_{\odot} \text{ yr}^{-1}$ , E+A systems at the high-luminosity end [ $M(z) < -22$ ] exhibit SFRs of greater than 300, and as high as  $2000 M_{\odot} \text{ yr}^{-1}$ . The SFRs are comparable to those found in LIRGs and ULIRGs at low redshift and our results indicate that massive LIRGs at low redshift could be the progenitors of massive E+A galaxies like those found in our sample.

We have performed a comprehensive study of the characteristics of the quenching that truncates the starburst in E+A galaxies. In particular, we have studied how the quenching efficiency varies as a function of galaxy mass and compared the results to scenarios where the quenching is due to SN and AGN, which are the typical sources of kinetic and thermal feedback invoked in galaxy formation models. We have found that in E+A galaxies with masses lesser than  $10^{10} M_{\odot}$ , quenching becomes less efficient as the galaxy mass increases. However, in galaxies with masses greater than  $10^{10} M_{\odot}$ , this trend is reversed and the quenching efficiency scales positively with galaxy mass. In terms of  $M(z)$  and stellar velocity dispersion ( $\sigma$ ), the reversal occurs at  $M(z) \sim -21$  and  $\sigma \sim 100 \text{ km s}^{-1}$ .

Since the mass threshold ( $10^{10} M_{\odot}$ ) where this reversal occurs is in excellent agreement with the mass above which AGN become significantly more abundant in nearby galaxies, these results can be qualitatively explained in terms of AGN and SN being the principal sources of feedback that quenches star formation in E+A

galaxies above and below  $M \sim 10^{10} M_{\odot}$ , respectively. In the absence of AGN ( $M < 10^{10} M_{\odot}$ ), the primary source of negative feedback are SN. As galaxies become more massive, the increasing depth of the potential well makes it more difficult to eject gas from the system, reducing the quenching efficiency. As a result, the quenching efficiency shows a negative correlation with galaxy mass. We have shown that simple energetic arguments, based on the assumption that quenching occurs through mechanical ejection of gas, are able to satisfy the observed properties of E+A galaxies with masses below  $10^{10} M_{\odot}$ . This indicates that, in these galaxies, the quenching is likely to be driven *purely* through mechanical feedback from SN.

Once they begin to appear ( $M > 10^{10} M_{\odot}$ ), AGN become the dominant source of energetic feedback. Given that the AGN luminosity scales with the mass of the BH ( $M_{\text{BH}}$ ) which, in turn, scales strongly with the central velocity dispersion  $\sigma$  as  $M_{\text{BH}} \sim \sigma^{4-5}$ , we expect AGN feedback to become more effective (and hence the quenching efficiency to increase) as the galaxy mass increases. We have shown that simple energetic arguments, based on the mechanical ejection of gas, indeed expect a positive correlation between the quenching efficiency and galaxy mass. However, the derived properties suggest that the quenching efficiencies rise an order of magnitude faster with galaxy mass than predicted by simple energetic arguments *that assume that the Eddington ratio does not vary as a function of host galaxy mass*. However, the correlation between quenching efficiency and galaxy mass can be reproduced if the Eddington ratio ( $\mu$ ) of the E+A galaxies is assumed to vary with  $M$  as  $M^{\gamma}$ , where  $1 < \gamma < 3$ . Since the E+A masses are spread over an order of magnitude, this implies that the Eddington ratios of the smallest AGN (with host galaxy masses  $M \sim 10^{10} M_{\odot}$ ) are roughly one-tenth of those for their most massive counterparts in this sample (if  $\gamma \sim 1$ ).

Finally, we have used our E+A sample to estimate the time it takes for galaxies to migrate from the blue cloud to red sequence. The persistent bi-modality in galaxy colours over a large range in redshift coupled with the build-up of the red sequence over time suggests that the net migration of galaxies from the blue cloud to the red sequence is an important feature of the macroscopic evolution of the galaxy population over time. The use of E+A galaxies, which have just truncated their star formation and are on the verge of this migratory transition, together with the use of both UV and optical photometry, produces reasonably robust estimates of the migration times. The migration times are estimated by ‘ageing’ the best-fitting SEDs of each E+A galaxy, keeping secondary parameters such as metallicity and  $E(B - V)$  constant throughout the migration. We calculate migration times between 1 and 5 Gyr, with a typical migration time of  $\sim 1.5$  Gyr.

The study of E+A galaxies arguably holds the key to understanding many of the processes that shape the evolution of galaxies. While our analysis is phenomenological in nature, this study has attempted to derive quantitative insights into some of these processes, especially the characteristics of feedback that is responsible for modulating and truncating star formation in galaxies. While many of the results derived here (e.g. time-scales over which AGN or SN feedback quenches star formation, the comparative efficiencies of the two feedback modes in potential wells of varying sizes or the migration times from the blue cloud to the red sequence) could prove useful constraints in galaxy formation models, future studies of E+A galaxies at high redshift are keenly anticipated because they will provide key insights into how such processes, that dictate the evolution of the galaxy population, evolve over time.

## ACKNOWLEDGMENTS

We are grateful to the anonymous referee for numerous insightful comments that improved the clarity of the original manuscript. The work presented in this paper would not have been possible without the Garching SDSS catalogue. SK is grateful to Christy Tremonti for many useful discussions regarding the extraction of spectroscopic parameters used in this study. Sven De Rijcke, James Binney, Lisa Young, Phillip Podsiadlowski and Sukyoung Yi are thanked for constructive comments.

SK acknowledges a Leverhulme Early-Career Fellowship, a BIPAC Fellowship and a Research Fellowship from Worcester College, Oxford. Part of the research presented in this study used the undergraduate computing facilities in the Department of Physics at Oxford.

Funding for the SDSS and SDSS-II has been provided by the Alfred P. Sloan Foundation, the Participating Institutions, the National Science Foundation, the U.S. Department of Energy, the National Aeronautics and Space Administration, the Japanese Monbukagakusho, the Max Planck Society and the Higher Education Funding Council for England. The SDSS web site is <http://www.sdss.org/>.

The SDSS is managed by the Astrophysical Research Consortium for the Participating Institutions. The Participating Institutions are the American Museum of Natural History, Astrophysical Institute Potsdam, University of Basel, University of Cambridge, Case Western Reserve University, University of Chicago, Drexel University, Fermilab, the Institute for Advanced Study, the Japan Participation Group, Johns Hopkins University, the Joint Institute for Nuclear Astrophysics, the Kavli Institute for Particle Astrophysics and Cosmology, the Korean Scientist Group, the Chinese Academy of Sciences (LAMOST), Los Alamos National Laboratory, the Max-Planck-Institute for Astronomy (MPIA), the Max-Planck-Institute for Astrophysics (MPA), New Mexico State University, Ohio State University, University of Pittsburgh, University of Portsmouth, Princeton University, the United States Naval Observatory and the University of Washington.

## REFERENCES

- Bekki K., Shioya Y., Couch W. J., 2001, *ApJ*, 547, L17
- Bell E. F. et al., 2004, *ApJ*, 608, 752
- Belloni P., Bruzual A. G., Thimm G. J., Roser H.-J., 1995, *A&A*, 297, 61
- Bernardi M., the SDSS Collaboration, 2003, *AJ*, 125, 1882
- Blake C., 2dF Collaboration, 2004, *MNRAS*, 355, 713
- Bondi H., Hoyle F., 1944, *MNRAS*, 104, 273
- Bower R. G., Lucey J. R., Ellis R., 1992, *MNRAS*, 254, 589
- Bressan A., Poggianti B., Franceschini A., 2001, in Márquez I., Masegosa J., del Olmo A., Lara L., García E., Molina J., eds, *QSO Hosts and Their Environments*. Kluwer, Dordrecht, p. 376
- Brinchmann J., Charlot S., White S. D. M., Tremonti C., Kauffmann G., Heckman T., Brinkmann J., 2004, *MNRAS*, 351, 1151
- Buyle P., Michielsen D., De Rijcke S., Pisano D. J., Dejonghe H., Freeman K., 2006, *ApJ*, 649, 163
- Chang T.-C., van Gorkom J. H., Zabludoff A. I., Zaritsky D., Mihos J. C., 2001, *AJ*, 121, 1965
- Couch W. J., Sharples R. M., 1987, *MNRAS*, 229, 423
- Cowie L. L., Songaila A., Hu E. M., Cohen J. G., 1996, *AJ*, 112, 839
- Dressler A., Gunn J. E., 1983, *ApJ*, 270, 7
- Fabricant D. G., McClintock J. E., Bautz M. W., 1991, *ApJ*, 381, 33
- Ferrarese L., Merritt D., 2000, *ApJ*, 539, L9
- Fukugita M., Hogan C. J., Peebles P. J. E., 1998, *ApJ*, 503, 518
- Galaz G., 2000, *AJ*, 119, 2118
- Gebhardt K. et al., 2000, *ApJ*, 539, L13

- Goto T., 2004, *A&A*, 427, 125  
 Goto T., 2005, *MNRAS*, 357, 937  
 Goto T., 2006, *MNRAS*, 369, 1765  
 Goto T., SDSS Collaboration, 2003, *PASJ*, 55, 771  
 Häring N., Rix H.-W., 2004, *ApJ*, 604, L89  
 Kauffmann G., SDSS Collaboration, 2003a, *MNRAS*, 341, 33  
 Kauffmann G. et al., 2003b, *MNRAS*, 346, 1055  
 Kaviraj S., GALEX Science Team, 2006a, accepted, *ApJ* (astro-ph/0601029)  
 (to appear in GALEX dedicated issue in December 2007)  
 Kaviraj S., Devriendt J. E. G., Ferreras I., Yi S. K., Silk J., 2006b, submitted  
 to *MNRAS* (astro-ph/0602347)  
 Kaviraj S., Rey S., Rich R. M., Lee Y., Yoon S., Yi S. K., 2007, *MNRAS*,  
 381, L74  
 Kennicutt R. C. Jr, 1998, *ApJ*, 498, 541  
 Liu C. T., Green R. F., 1996, *ApJ*, 458, L63  
 Liu C. T., Hooper E. J., O'Neil K., Thompson D., Wolf M., Lisker T., 2007,  
*ApJ*, 658, 249  
 Martin D. C., GALEX Collaboration, 2005, *ApJ*, 619, L1  
 Mihos J. C., Hernquist L., 1994, *ApJ*, 437, L47  
 Miller N. A., Owen F. N., 2001, *ApJ*, 554, L25  
 Norton S. A., Gebhardt K., Zabludoff A. I., Zaritsky D., 2001, *ApJ*, 557, 150  
 Poggianti B. M., Wu H., 2000, *ApJ*, 529, 157  
 Poggianti B. M., Bressan A., Franceschini A., 2001, *ApJ*, 550, 195  
 Quintero A. D. et al., 2004, *ApJ*, 602, 190  
 Sanders D. B., Mirabel I. F., 1996, *ARA&A*, 34, 749  
 Shankar F., Lapi A., Salucci P., De Zotti G., Danese L., 2006, *ApJ*, 643, 14  
 Smail I., Morrison G., Gray M. E., Owen F. N., Ivison R. J., Kneib J.-P.,  
 Ellis R. S., 1999, *ApJ*, 525, 609  
 Tran K.-V. H., Franx M., Illingworth G. D., van Dokkum P., Kelson D. D.,  
 Magee D., 2004, *ApJ*, 609, 683  
 Tremonti C. A. et al., 2004, *ApJ*, 613, 898  
 Wang J. L., Xia X. Y., Mao S., Cao C., Wu H., Deng Z. G., 2006, *ApJ*, 649,  
 722  
 Yang Y., Zabludoff A. I., Zaritsky D., Lauer T. R., Mihos J. C., 2004, *ApJ*,  
 607, 258  
 Yi S. K., 2003, *ApJ*, 582, 202  
 Yi S. K., GALEX Science Team, 2005, *ApJ*, 619, L111  
 Zabludoff A. I., Zaritsky D., Lin H., Tucker D., Hashimoto Y., Sheckman  
 S. A., Oemler A., Kirshner R. P., 1996, *ApJ*, 466, 104

This paper has been typeset from a  $\text{\TeX/L\AA\TeX}$  file prepared by the author.